Journal of Nanoparticle Research (2005) 7: 227–236
DOI: 10.1007/s11051-005-4270-6

Spectroscopic studies on nanodispersions of CdS, HgS, their core-shells and composites prepared in micellar medium

Indranil Chakraborty, Debolina Mitra and Satya P. Moulik
Department of Chemistry, Centre for Surface Science, Jadavpur University, Kolkata, 700 032, India (E-mail: spmcss@yahoo.com)

Received 15 February 2005; accepted in revised form 21 March 2005

Key words: CdS, HgS dispersions, co-colloids, core-shell products, CTAB, optical enhancement, particle characterization

Abstract

CdS is a large band gap material compared to HgS. Both are interesting from academic and technological points of view. The nanodispersions (colloids) of CdS and HgS as well their core-shell products and composites (co-colloids) were prepared by varied modes of precursor addition in micellar solution of cationic surfactant cetyltrimethylammonium bromide (CTAB). The prepared dispersions were studied by spectroscopic and electron microscopic techniques.

Introduction

Nanomaterials are emerging very fast in the field of material science in recent years owing to strong and fruitful coupling between basic and applied research. The unusual photophysical properties of metal and semiconductor nanomaterials impart importance to their industrial applications by virtue of their size tunable band gaps. On photo irradiation, an electron is promoted from the valence band creating a vacancy or hole. Large crystals (with bulk band gap value) often contain several electron-hole pairs under electrical or optical excitation, which at room temperature dissociate. In a small crystallite, generally one electron-hole pair (called exciton) is present, and is subjected to the spatial restriction, which prevents its dissociation. The electron and the hole in the pair interact by way of Coulomb forces, exchange forces and polarization of the lattice vibrations (Brus, 1998). The imposed spatial restriction on decreasing particle size increases the energy of separation between the ground and the excited electronic states as expected from the particle in an infinite potential well model which results in the blue shift of the absorption peak with enhancement of optical band gap of the material compared to the bulk phase. This is known as quantum confinement effect (Wang & Herron, 1991; Alivisatos, 1996). The density of states in valence and conduction bands continually varies with energy of the electronic states, which in nanomaterials breaks up into a collection of discrete density of states (DOS) over the entire energy spectrum (Wise, 2000). As a consequence, absorption and fluorescence intensities increase with decreasing particle size.

Insoluble dispersions in a medium tend to coagulate to minimize surface free energy. In nanomaterial synthesis, this natural tendency may be opposed by using rigid or semirigid templates like glass (Battisha, 2002), zeolites (Wang & Herron, 1987), molecular sieve (Abe et al., 1995), gel (Chakraborty & Moulik, 2004), polymer (Wang et al., 1987; Qi et al., 2001), membrane (Pattabi & Uchil, 2003; ibid., 2000) , etc. Other methods like vapor phase reaction, electrochemical deposition

etc. are also used. The water pool of water-in-oil microemulsion as a microreactor is convenient for preparation of nanomaterials (Pileni, 1993; Chakraborty & Moulik, 2005). Although micellar solution has long been reported as a suitable template for preparation of metal nanomaterials, it has been scarcely used for the preparation of compounds. Recently, we have reported the preparations of PbS (Chakraborty & Moulik, 2004), ZnS (Mitra et al., in press) and CoS_2 (Chakraborty et al., communicated) nanomaterials in micellar medium of AOT, SDS and CTAB respectively. The materials prepared in solution phase, however, require some surface-stabilizing agent which offer a hydrophobic repulsion barrier towards particle coagulation as well as they passivate the defect structure present on the surface of the material. These defect structures efficiently decrease the emission quantum yield by way of radiationless trapping process. The surface-passivating agents block the defect structure and help to increase the emission efficiency.

The organometallic route of preparing fairly monodisperse nanomaterials under annealed condition has been reported (Murray et al., 1993). Overcoating nanomaterials by inorganic shell structure provides more robust capping than the organically passivated analogue. Coating of semiconductor nanomaterials by higher band gap inorganic material produces improved photoluminescence properties due to passivated surface nonradiative recombination sites (Dabbousi et al., 1997). They have prepared CdSe–ZnS nanocomposite via organometallic route and explained the continuous variation in color of the composite over the entire visible light depending on the size of the CdSe core. The photo darkening and electro darkening of the same material have also been studied by Rodriguez-Viejo et al. (2000). Synthesis of $Cd_{1-x}Zn_xS$ via sol-gel route in silica matrix (Bhattacharjee et al., 2002) has also been reported. Elliot et al. (1999) have reported the CdS–HgS composite in Langmuir–Blodgett (LB) films (Elliot et al., 1999). Joshi et al. (2003) have reported the growth of $Pb_{1-x}Fe_xS$ on quartz surface. Qi et al. (1996) have reported the preparation and characterization of CdS–HgS composite in reverse micellar medium. ZnS passivated CdS particles have also been prepared by Hsu and Lu (2004) by metal-organic chemical vapor deposition (MOCVD) process. The couple composite of CdS–CdSe and core-shell type (CdS)CdSe and (CdSe)CdS nanomaterials stabilized by polyphosphate have been also reported by Tian et al. (1996). Weller and his coworkers have made extensive study on double-decker CdS–HgS and triple-decker CdS–HgS–CdS colloidal dispersions in polyphosphate solution (Hasselbarth et al., 1993; Mews et al., 1994; Schooss et al., 1994; Porteanu et al., 2001; Braun et al., 2002).

CdS is a well-studied semiconductor because of its stability, easy preparation and distinct band gap that helps to detect a number of optical phenomena. Organically passivated CdS has been extensively studied (Miyake et al., 1999; Fogila et al., 2001; Kolny et al., 2002; Torimoto et al., 2003). Although HgS nanoparticle is very useful in ultrasonic transducer, image sensors, electrostatic image material, photoelectric conversion devices (Tokyo, 1975, 1978; Tokyo & Azkio, 1978) and infrared sensor (Higginson et al., 2002), reports on nano-HgS are relatively less (Zhu et al., 2000; Bhattacharjee et al., 2002; Pal et al., 2003; Shao et al., 2003; Wang & Zhu, 2004).

In this paper, we report the preparation and characterization of pure nanoparticles of CdS and HgS, and their core-shell products and composites in micellar medium of the cationic surfactant cetyltrimethylammonium bromide (CTAB). HgS is a small band gap material with bulk band gap 0.5 eV, whereas CdS has a comparatively large band gap of 2.5 eV. The materials have similar lattice constants (Hasselbarth et al., 1993) that facilitate efficient formation of co-colloid. The co-colloids and core shell products with a maximum of [HgS] remained stabilized in micellar solution for 2–3 days and thereafter precipitated out; the rest, however, remained in solution for weeks. The reversibility of this precipitation was very striking. The redispersed co-colloidal solution has shown better stability compared to its stability at the initial stage of its formation.

Experimental section

Materials and methods

The surfactant CTAB used was AR grade product of Aldrich, USA. $CdCl_2$ and $HgCl_2$ were AR grade products of Loba and BDH, India, respectively.

Na_2S was an AR grade product of L.C. Pvt. Ltd (India). All the reagents were used as received. All solutions were prepared in doubly distilled water and filtered through 0.22 μ millipore filter paper.

UV spectra were measured with a Shimadzu (Japan) 160A spectrophotometer operating in dual beam mode in quartz cells of 5 mm path length. Fluorescence spectra were measured with Shimadzu (Japan), R.F. spectrofluorimeter. TEM measurements were taken in a Hitachi (Model H-600) instrument (Japan). For TEM experiments, dispersions were deposited on carbon coated Cu grids, dried by simple evaporation, and an accelerating voltage of 50 kV was used.

Synthesis of pure nanoparticles

Aqueous micellar solution of CTAB at 10 mM (cmc 1 mM) was prepared in doubly distilled water. 0.1 M aqueous $CdCl_2$ or $HgCl_2$ solution was then added with a Hamilton microsyringe into 5 ml of the CTAB solution. It was thoroughly mixed and freshly prepared 0.2 M Na_2S solution was further added into the solution to yield 1:1 mole ratio. The CdS nanocrystals formed in the micellar medium were yellow and the HgS nanocrystals were black in color. The concentration of the $CdCl_2$ or $HgCl_2$ in the experiments was varied in the range of 0.1–0.5 mM to form varied concentrations of the products. For core shell products, Na_2S was added in $CdCl_2$ solution in excess of stoichiometric composition. After the formation of the CdS, $HgCl_2$ solution was slowly added under stirring condition for complete formation of HgS supposed to be deposited mainly on CdS particle surface. Following a similar protocol HgS (core)–CdS (shell) product was synthesized. The addition of Na_2S into a mixed electrolyte solution of $CdCl_2$ and $HgCl_2$ led to the formation of CdS and HgS co-colloids (CdS–HgS). In each preparation, the Cd^{2+}:Hg^{2+} mole ratio was varied as 5:1, 3:2, 1:1, 2:3 and 1:5. The core-shell products obtained from CdS and HgS are designated as CdS/HgS and HgS/CdS where the numerators in the ratios are shells and denominators are cores.

Absorption spectroscopy

$CdCl_2$ and $HgCl_2$ in aqueous solution do not absorb in the u.v.–vis region. CTAB solution absorbs with a maximum at 300 nm that remains unaltered on addition of $CdCl_2$ and $HgCl_2$. CdS in CTAB medium has shown an absorption shoulder in the

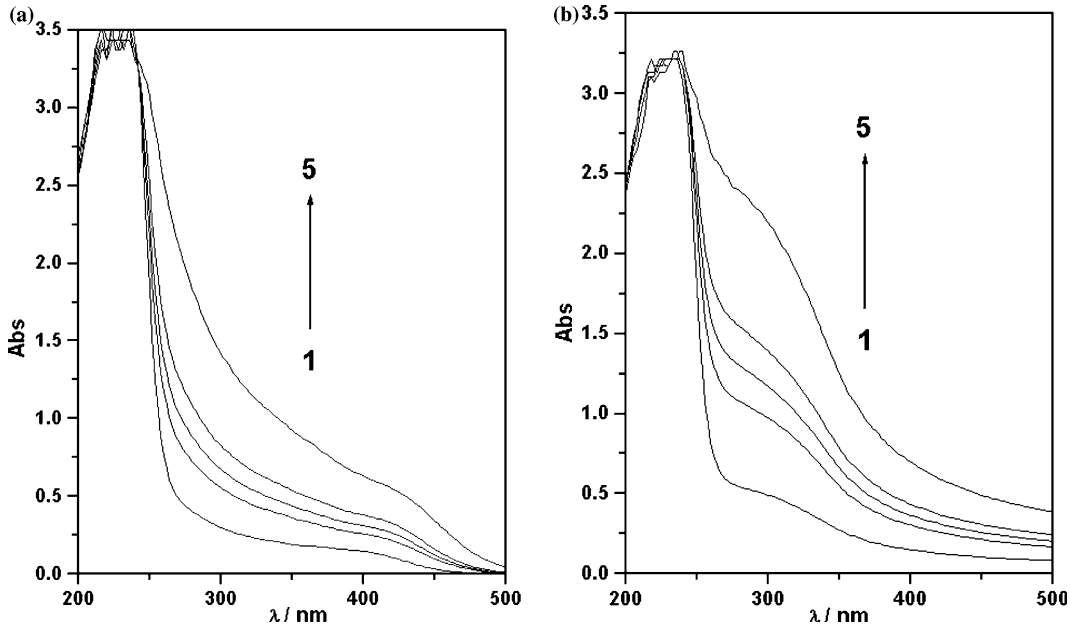

Figure 1. Absorption spectra of (a) CdS and (b) HgS nanoparticles with varying concentration in 10 mM CTAB solution. (a) curve 1, 0.1 mM; 2, 0.2 mM; 3, 0.25 mM; 4, 0.3 mM; 5, 0.5 mM. (b) same as in a.

range of 400–430 nm with variation of [CdS] from 0.1 to 0.5 mM (Figure 1a). This is due to the 1s–1s (HOMO-LUMO or excitonic) transition (Mews et al., 1994). The nano-dispersion of $HgCl_2$ in CTAB medium has absorbed with a shoulder ranging from 302 to 315 nm when $HgCl_2$ was varied from 0.1 to 0.5 mM (Figure 1b). The blue shift of the absorption shoulder (from 430 to 400 nm) and the corresponding increase in the molar absorptivity (ε) with decreasing [CdS] are profiled in curves 1 and 2 respectively in Figure 2a. Such results on the absorption shoulder (blue shift from 315 to 302 nm) and the molar absorptivity with decreasing [HgS] are exemplified in curves 1 and 2 respectively in Figure 2b. The spectral shifts and the corresponding changes in ε can be explained on the basis of quantum confinement effect.

At a fixed [CTAB] in the medium, the particle size in the nanodispersions decreased with decreasing [CdS] and [HgS]. With decreasing particle size, the spatial restriction imposed on the photogenerated electron in the conduction band increased and in the limit of the particle size where this restriction was of the order of the de Brogli wavelength, called the Bohr excitonic radius, $a_B = (\hbar^2 p)/(e^2 m^*)$ of the electron-hole pair (where

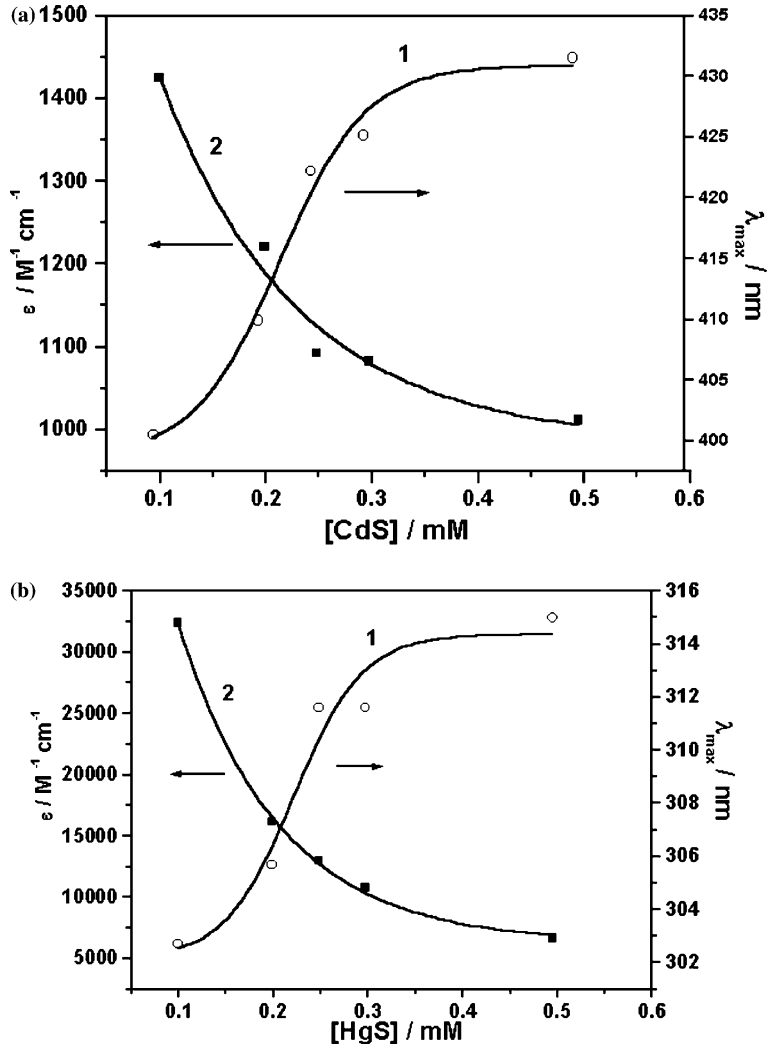

Figure 2. Concentration dependent shift in the spectral shoulder and molar absorptivity of the CdS and HgS nanomaterials prepared in 10 mM CTAB medium. (a) (CdS): curve 1, shift in shoulder. curve 2, changes in ε. (b) (HgS): curve 1 and 2, as in a.

the terms h = Planck constant/2π, p is the permittivity and e is the electronic charge), there was a dramatic change in photophysical properties of the colloids. In such a situation, it can be considered that an electron is confined within an infinite potential well with the energy,

$$E_n = (n^2h^2/8\,m^*L^2) \tag{1}$$

where, m^* and L are respectively the effective mass of the electron/hole/exciton and the length scale over which the photogenerated electron is free to move. Thus, the blue shift arose due to decreasing particle size on decreasing [CdS] as expected from easier stabilization (greater number of colloidal dispersion and lesser tendency of coagulation down the concentration ladder). On decreasing particle size, the continuous variation of density of states (DOS) over the energy ladder was splitted up into a number of discrete states. To maintain constancy of the 1:1 correspondence of the number of excitations with the number of absorbed photons as compared to the bulk, the number of transitions (in the particular energies) rich in DOS increased leading to optical enhancement effect.

The band gaps of the nanodispersions were calculated using the (Tauc & Menth, 1972) equation as done earlier (Chakraborty & Moulik, 2000, 2004; Chakraborty & Moulik, 2005)

$$(\varepsilon h\nu)^2 = P(E_g - h\nu) \tag{2}$$

where ε, h, ν, E_g and P are the molar extinction coefficient, Planck Constant, frequency of light, band gap of the nanoparticle and an arbitrary constant respectively. The linear part of the $(\varepsilon\, h\, \nu)^2$ vs. $h\,\nu$ plot was considered for the evaluation of E_g (Figure 3a, b). Nonlinearity in the higher wavelength region arose from some indirect transitions and/or polydispersity in particle dimension. The calculated band gap values varied in the range of 4.37–4.87 eV for CdS, and 4.26–4.86 eV for HgS. The variation of band gap for both the preparations with concentration has followed the relation, $E_g = a + b_1$[dispersion] + b_2[dispersion]^2 ([dispersion] expressed in M) with values of the constants a, b_1, and b_2 as 4.822, 779.15 and -3.44×10^6 respectively for CdS and 4.821, 663.31, and -3.629×10^6 respectively for HgS. The graphical illustrations are depicted in Figure 3c.

The size of the prepared particles in the nanodispersion was also calculated from the spectral data using Wang equation (Wang et al., 1987)

$$\Delta E = (\hbar^2\pi^2/2R^2)(1/m_e + 1/m_h) - 1.8e^2/\mathrm{p}R \tag{3}$$

which reduces to

$$E = [E_g^2 + 2E_gh^2(\pi/R)^2/m*]^{1/2} \tag{4}$$

for materials with a predominant ionic character. In equation (3), $\Delta E = E_g - E$, E is the bulk band gap and R is the radius of the particle, m_e is the mass of an electron, m_h is the mass of the hole, p is the permittivity and the rest of the terms have been already defined.

We have calculated the diameter from absorption study, d_{abs} ($2R$) of CdS and HgS using Equation (4) with $m_e = 0.2m_0$ and $m_h = 0.7m_0$ for CdS (Tian et al., 1996), for mercuric sulfide the values were $m_e = 0.036\ m_0$ and $m_h = 0.044\ m_0$ [30], (m_0 is the rest mass of an electron). The results are shown in Tables 1 and 2.

For the core-shell materials and co-colloids (composites), the total concentration of the semiconductor products was maintained constant (see legends Figure 4a–c) but the CdS to HgS mole ratio was varied. For the CdS/HgS and HgS/CdS core-shell materials at mole ratio 5:1 (Figure 4a), the shoulder for CdS peak appeared at 436 and 440 nm respectively. The red shift of the shoulder compared to pure CdS was greater for the product with CdS forming the core. The absorbance of the materials at λ = 400 nm have followed HgS/CdS > CdS/HgS > CdS. The increased absorbance compared to the pure sample was due to the leakage of the photogenerated electron of CdS to the HgS shell and *vice versa* (Dabbousi et al., 1997). The spectral feature of HgS was absent in both core-shell products. However, the co-colloid at CdS:HgS mole ratio 5:1 has evidenced the spectral feature of the deficient compound HgS at around 290 nm.

The core-shell and composite samples with CdS:HgS of mole ratio 3:2 and 2:3 produced almost featureless spectra over the entire u.v.–vis region with increased intensity reflecting formation of some newer electronic states compared to the

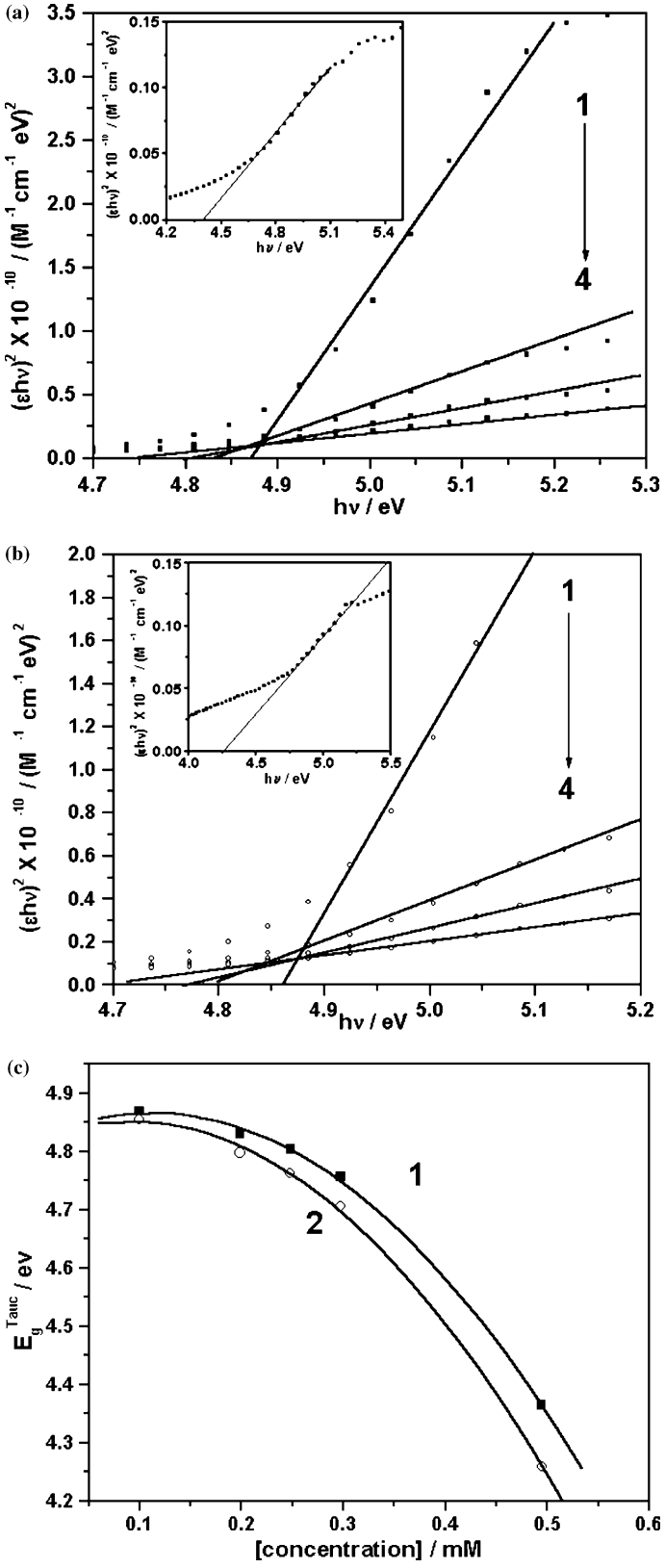
(a)
(εhν)² X 10 ⁻¹⁰ / (M⁻¹cm⁻¹ eV)²
hν / eV
1
4
(εhν)² X 10 ⁻¹⁰ / (M⁻¹ cm⁻¹ eV)²
hν / eV
(b)
(εhν)² X 10 ⁻¹⁰ / (M ⁻¹ cm⁻¹ eV)²
hν / eV
1
4
(εhν)² X 10 ⁻¹⁰ / (M⁻¹ cm⁻¹ eV)²
hν / eV
(c)
E_g^Tauc / ev
[concentration] / mM
1
2

Figure 3. Tauc plot for the determination of the band gap of CdS and HgS. (a) (CdS): curve 1, 0.1 mM; 2, 0.2 mM; 3, 0.25 mM; 4, 0.3 mM. Inset [CdS] = 0.5 mM. (bulk band gap is 2.5 eV). (b) (HgS): curves identification as in a. (bulk band gap is 0.5 eV). (c) Dependence of E_g on the concentration of CdS and HgS. Curve 1, CdS; 2, HgS.

individuals. The spectrum at 1:1 mole ratio is presented in Figure 4b for an illustration.

In the system containing CdS:HgS at mole ratio 1:5 (Figure 4c), the spectral shoulder for CdS was absent both CdS/HgS and HgS/CdS core-shell samples. The HgS shoulder at 292 nm was observed in both the samples. Unlike the 5:1 system discussed above, no shift of the HgS shoulder was observed here; however, the absorbance at $\lambda = 300$ nm followed the order HgS/CdS > CdS/HgS > HgS as observed for the 5:1 mole ratio. The co-colloid (CdS–HgS) also evidenced the spectral feature of the deficient component CdS with the shoulder at 400 nm. When all these systems were illuminated with a He–Ne laser operating at 632 nm, no change in the absorption spectra was observed; the materials were not photo bleached by the laser radiations.

Fluorescence spectroscopy

Fluorescence spectra of the CdS nanocrystallites prepared in 10 mM CTAB solution have witnessed a peak at 616 nm (Figure 5) when excited at 350 nm and the fluorescence intensity decreased with decreasing [CdS]. This band is assigned to the radiative recombination of free electrons and holes following the model of rapid trapping and detrapping of the charge carriers (Eychmuller et al., 1991). Large nanocrystals with band gap close to the bulk value containing several electron hole pairs resulted (under electrical or optical excitation conditions); at room temperature they undergo dissociation and their recombination is a many body kinetic problem as in the bulk. Small nanocrystals normally contain one electron hole pair, which cannot dissociate since the electron and hole are restrictedly confined in the crystal domain. They, therefore, interact with each other by the Coulomb and exchange forces and via polarization of lattice vibrations. This is essentially the molecular excited state that decays by unimolecular process.

The CdS samples prepared from concentration lower than 0.25 mM have evidenced no fluorescence. This is because the particles formed were very small with large number of defect sites, which acted as efficient traps for electron/hole/exciton resulting in a decrease in feeble radiative emission or negligible fluorescence. At 350 nm excitation, pure HgS nanodispersions did not emit. The core shell materials of HgS/CdS and CdS/HgS and the co-colloids showed no emission features. This was a significant result evidencing alteration of emission characteristics on cohabitation. Otherwise, as in quenching, the fluorescence intensity would have been quenched in a gradual way on increasing HgS mole ratio in the samples. In case of pure CdS, after light absorption the photogenerated electrons were quickly trapped in shallow traps on the surface of the nanoparticles from where they might be detrapped into the conduction band, giving rise to the delayed excitonic fluorescence of the CdS nanocrystals. On addition of HgS nanoparticles, hole transfer from the CdS to the HgS valence band has been considered to be much faster than the fluorescence in the CdS moiety and hence no CdS fluorescence was observed in the core shells and the co-colloids.

Transmission electron microscopy

The TEM micrograms have evidenced formation of spherical to prolate particles, in general, which also aggregated in complex network form. Rod shaped aggregate formation was also observed

Table 1. Optical band gap and diameter of CdS nanoparticles at different product concentration

[CdS]/mM	0.1	0.2	0.25	0.3	0.5
E_g/eV	4.87	4.83	4.80	4.75	4.37
d_{abs}/nm	2.03	2.05	2.06	2.09	2.29

Table 2. Optical band gap and diameter of HgS nanoparticles at different product concentration

[HgS]/mM	0.1	0.2	0.25	0.3	0.5
E_g/eV	4.86	4.80	4.76	4.71	4.26
d_{abs}/nm	4.17	4.20	4.22	4.25	4.49

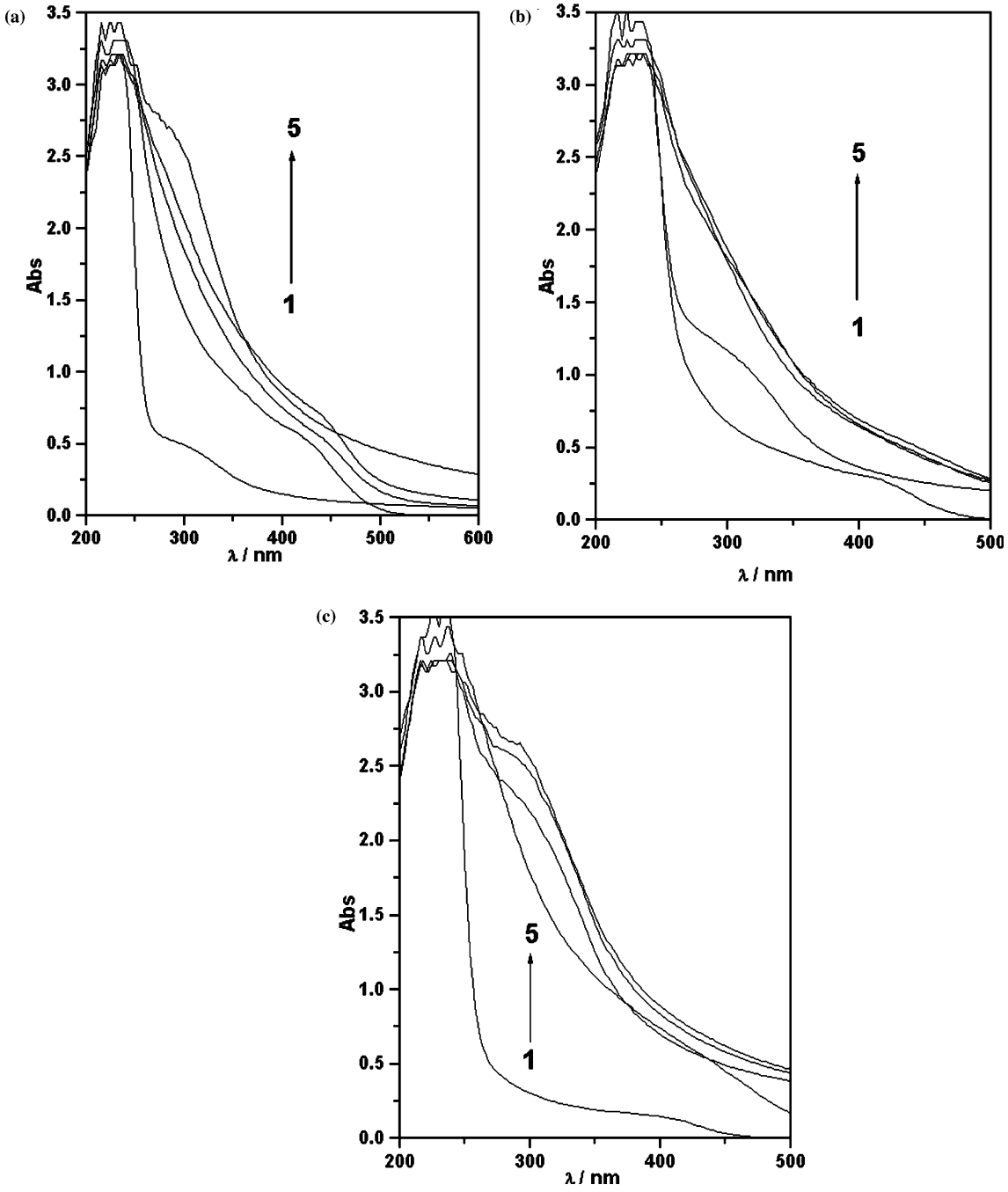

Figure 4. Absorption spectra of nanomaterials of CdS, HgS their core-shells and composites prepared in 10 mM CTAB medium. (a) (CdS:HgS = 5:1, at λ = 400 nm): 1, pure HgS at 0.1 mM; 2, pure CdS at 0.5 mM; 3, CdS/HgS ([CdS] = 0.5 mM, [HgS] = 0.1 mM); 4, CdS–HgS ([CdS] = 0.5 mM, [HgS] = 0.1 mM); 5, HgS/CdS ([CdS] = 0.5 mM, [HgS] = 0.1 mM). (b) (CdS:HgS = 1:1, at λ = 400 nm): 1, pure CdS (0.25 mM); 2, pure HgS (0.25 mM); 3, CdS–HgS ([CdS] = 0.25 mM, [HgS] = 0.25 mM); 4, CdS/HgS ([CdS] = 0.25 mM, [HgS] = 0.25 mM); 5, HgS/CdS ([CdS] = 0.25 mM, [HgS] = 0.25 mM). (c) (CdS:HgS = 1:5, at λ = 300 nm): 1, pure CdS at 0.1mM; 2, CdS–HgS ([CdS] = 0.1 mM, [HgS] = 0.5 mM); 3, pure HgS at 0.5 mM; 4, CdS/HgS ([CdS] = 0.1 mM, [HgS] = 0.5 mM); 5, HgS/CdS ([CdS] = 0.1 mM, [HgS] = 0.5 mM).

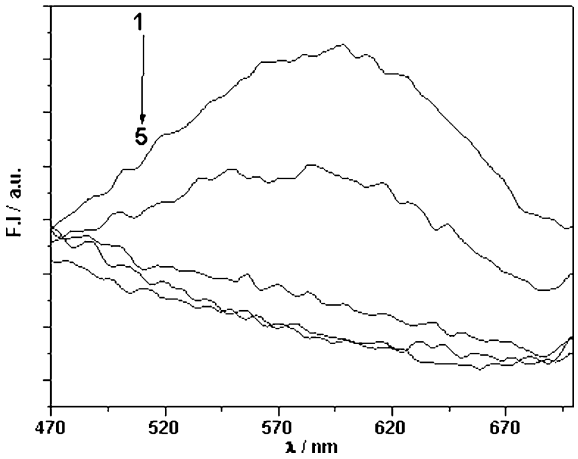

Figure 5. Fluorescence spectra of nanodispersion of CdS in 10 mM CTAB (Excitation wavelength = 350 nm). Curve 1, 0.5 mM; 2, 0.3 mM; 3, 0.25 mM; 4, 0.2 mM; 5, 0.1 mM.

particularly in co-colloidal systems (Figure 6a). The core-shell particles also produced network structure. The HgS/CdS core-shell particles formed isolated nearly monodisperse, prolate particles (Figure 6b). For the CdS/HgS particles, tendency of formation of needle shaped primary aggregates prevailed which ended up into three-dimensional assemblies (Figure 6c). The average diameter of the core shell and the co-colloids as obtained from TEM are given in Table 3.

Table 3. Average TEM diameters for the core shells and the co-colloids at various mole ratios of CdS and HgS

Shape	CdS/HgS Spherical	CdS–HgS Cylindrical		HgS/CdS Spherical
Mole ratio (CdS:HgS)	d_{TEM}/nm	Length/nm	Width/nm	d_{TEM}/nm
5:1	5.6	6.0	2.0	5.8
3:2	5.4	5.9	1.9	5.6
1:1	5.4	5.6	1.6	5.5
2:3	5.5	5.9	1.6	5.6
1:5	5.8	6.2	2.3	6.0

Conclusions

The band gap of CdS within a concentration range of 0.1–0.5 mM varied within 4.87–4.37 eV, while that for HgS prepared in the same concentration range varied within 4.86–4.26 eV. The formation of core shell particles have been evidenced in the uv-vis and fluorescence spectra. The absorbance spectra of the co-colloids in the two extreme composition range evidenced feature of the deficient compound. The spectral feature of the co-colloids

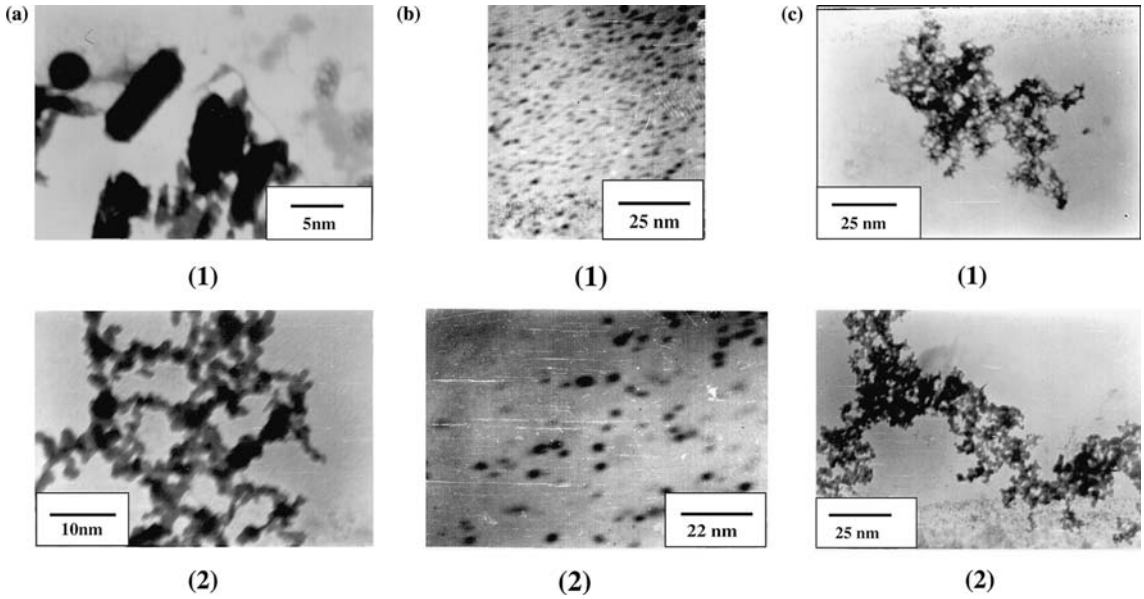

Figure 6. Transmission electron micrograph of the core-shells and composites of CdS and HgS (a) CdS–HgS at CdS:HgS mole ratio 1, 5:1; 2, 1:5. (b) HgS/CdS at CdS:HgS mole ratio 1, 5:1; 2, 1:5. (c) CdS/HgS at CdS:HgS mole ratio 1, 2:3; 2, 3:2.

and the core shell composites were significantly different from pure samples. The CdS nanoparticles formed at [CdS] > 0.25 mM evidenced an emission peak at 616 nm. The pure HgS nanoparticles did not fluoresce. The co-colloids and the core shells also did not fluoresce; the emission characteristics were altered due to cohabitation. Rod shaped aggregates in the co-colloidal systems and network structure in the core shell products indicated formation of two kinds of nanoparticles by the two modes of preparation procedure.

Acknowledgements

IC and DM thanks CSIR, Government of India for financial assistance during the work and SPM thanks INSA, Government of India, for a Senior Scientist position.

References

Abe T., Y. Tachibana, T. Uematsu & M. Iwamoto, 1995. J. Chem. Soc. Chem. Commun. 1617.
Alivisatos A.P., 1996. Science 271, 933–937.
Battisha I.K., 2002. Coden Fizae 461–70.
Bhattacharjee B., S.K. Mandal, K. Chakrabarty, D. Ganguly & S. Chaudhury, 2002. J. Phys. D Appl. Phys. 35, 2636–2642.
Braun M., S. Link, C. Burda & M. El-Sayed, 2002. Chem. Phys. Lett. 36, 446–452.
Brus L.E., 1998. J. Phys. Chem. Solids 59, 459–465.
Chakraborty I. & S.P. Moulik, 2004. J. Disp. Sci. Technol. 25, 849–859.
Chakraborty I. & S.P. Moulik, 2004. J. Nanopart. Res. 6, 233–240.
Chakraborty I. & S.P. Moulik, 2005. J. Nanopart. Res. 7, 237–247.
Chakraborty I., P.K. Malik & S.P. Moulik, communicated.
Dabbousi B.O., J. Rodriguez-Viejo, F.V. Mikulec, J.R Heine, H. Mattoussi, R. Ober, K.F. Jensen & M.G. Bawendi, 1997. J. Phys. Chem. B 101, 9463–9475.
Elliot D.J., D.N. Furlong & F. Grieser, 1999. Colloid Surf. A 155, 101–110.
Eychmuller A., A. Hasselbarth, L. Katsikas & H. Weller, 1991. Ber. Bunsen-Ges. Phys. Chem. 95, 79–85.
Foglia S., L. Suber & M. Righini, 2001. Colloid Surf. A 177, 3–12.
Hasselbarth A., A. Eychmullar, R. Eichberger, M. Giersig, A. Mews & H. Weller, 1993. J. Phys. Chem. 97, 5333–5340.
Higginson K.A., M. Kuno, J. Bonevich, S.B. Quardi, M. Yousuf & H. Mattoussi, 2002. J. Phys. Chem. B 106, 9982 .
Hsu Y-J. & S-Y. Lu, 2004. Langmuir 20, 194–201.
Joshi R.K., A. Kanjilal & H.K. Sehgal, 2003. Nanotechnology 14, 809–812.
Kolny J., A. Kornowski & H. Weller, 2002. Nano. Lett. 2, 361–364.
Mews A., A. Eychmuller, M. Giersig & H. Weller, 1994. J. Phys. Chem. 98, 934–941.
Mitra D., Chakraborty I., Moulik S.P., Colloid Journal. in press.
Miyake M., T. Torimoto, T. Sakata, H. Mori & H. Yoneyama, 1999. Langmuir 15, 1503–1507.
Murray C.B., D.J. Norris & M.G. Bawendi, 1993. J. Am. Chem. Soc. 115, 8706–8715.
Pal B., S. Ikeda & B. Ohtani, 2003. Inorg. Chem. 42, 1518–1524.
Pattabi M. & J. Uchil, 2003. Solar Ener. Mater. Solar Cells 76, 323–330.
Pattabi M. & J. Uchil, 2000Solar Energy Mater. Solar Cells 63, 309–314 .
Pileni M.P., 1993. J. Phys. Chem. 97, 6961–6973.
Porteanu H.E., E. Lifshitz, M. Pflughoefft, A. Eychmuller & H. Weller, 2001. Phys. Stat. Sol. b 226, 219–232.
Qi L., J. Ma, H. Cheng & Z. Zhao, 1996. Colloid Surf. A 111, 195–202.
Qi L., H. Colfen & M. Antonietti, 2001. Nano. Lett. 1, 61–65.
Rodriguez-Viejo J., H. Mattoussi, J.R. Heine, M.K. Kuno, J. Michel, M.G. Bawendi & K.F. Jensen, 2000. J. Appl. Phys. 87, 8526–8534.
Rollins H.W., T. Whiteside, G.J. Shafer, J-J. Ma, M-H. Tu, J-T. Liu, D.D. DesMarteau & Y-P. Sun, 2000. J. Mater. Chem. 10, 2081–2084 .
Shao M., L. Kong, Q. Li, W. Yu & Y. Qian, 2003. Inorg. Chem. Comm. 6, 737–739.
Schooss D., A. Mews, A. Eychmuller & H. Weller, 1994. Phys. Rev. B 49, 17072–17078.
Tauc J. & A. Menth, 1972. J. Non-Cryst. Sol. 269, 8–10.
Tian Y., T. Newton, N.A. Kotov, D.M. Guldi & J.H. Fendler, 1996. J. Phys. Chem. 100, 8927–8939.
Tokyo N., 1975. Jpn Kokai Pat. 75130378 (C1.H01L.C01B).
Tokyo N. & K. Azkio, 1978. Jpn Kokai Pat. 7855478(C1.C23C15/00).
Tokyo N., 1978. J. Appl. Phys. 46, 4857–4862.
Torimoto T., J.P. Reues, K. Iwasaki, B. Pal, T. Shibayama, K. Sugawara, H. Takahashi & B. Ohtani, 2003. J. Am. Chem. Soc. 125, 316–317.
Wang Y. & N. Herron, 1987. J. Phys. Chem. 91, 854 .
Wang Y. & N. Herron, 1991. J. Phys. Chem. 95, 525–532.
Wang Y., S. Suna, W. Mahler & R. Kasowski, 1987. J. Chem. Phys. 87, 7315–7322.
Wang H. & J-J. Zhu, 2004. Ultrasonics Chem. 11, 293–300.
Wise F.W., 2000. Acc. Chem. Res. 33, 773–780.
Zhu J., S. Liu, O. Palchik, Y. Koltypin & A. Gedanken, 2000. J. Colloid Interf. Sci. 153, 342–348.